Environmental Science & Technology

Article

pubs.acs.org/est

Core–Shell Structure Dependent Reactivity of $Fe@Fe_2O_3$ Nanowires on Aerobic Degradation of 4-Chlorophenol

Zhihui Ai,[†] Zhiting Gao,[†] Lizhi Zhang,[†,*] Weiwei He,[‡] and Jun Jie Yin[‡]

[†]Key Laboratory of Pesticide & Chemical Biology of Ministry of Education, Institute of Environmental Chemistry, College of Chemistry, Central China Normal University, Wuhan 430079, People's Republic of China

[‡]Center for Food Safety and Applied Nutrition, Food and Drug Administration, College Park, Maryland 20740, United States

Ⓢ *Supporting Information*

ABSTRACT: In this study, core–shell $Fe@Fe_2O_3$ nanowires with different iron oxide shell thickness were synthesized through tuning water-aging time after the reduction of ferric ions with sodium borohydride without any stirring. We found that these $Fe@Fe_2O_3$ nanowires exhibited interesting core–shell structure dependent reactivity on the aerobic degradation of 4-chlorophenol. Characterization results revealed that the core–shell structure dependent aerobic oxidative reactivity of $Fe@Fe_2O_3$ nanowires was arisen from the combined effects of incrassated iron oxide shell and more surface bound ferrous ions on amorphous iron oxide shell formed during the water-aging process. The incrassated iron oxide shell would gradually block the outward electron transfer from iron core for the subsequent two-electron molecular oxygen activation, but more surface bound ferrous ions on iron oxide shell with prolonging aging time could favor the single-electron molecular oxygen activation, which was confirmed by electron spin resonance spectroscopy with spin trap technique. The mineralization of 4-chlorophenol was monitored by total organic carbon measurement and the oxidative degradation intermediates were analyzed by gas chromatography–mass spectrometry. This study provides new physical insight on the molecular oxygen activation mechanism of nanoscale zerovalent iron and its application on aerobic pollutant removal.

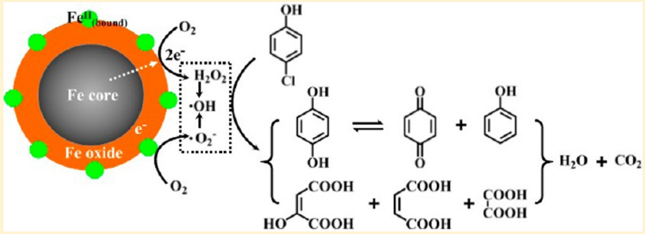

INTRODUCTION

Iron and its oxides are ubiquitous and profoundly influence the environment through redox cycling of iron.[1] In view of natural abundance and environmental benignancy of iron, the utilization of iron redox cycling for environmental remediation is very attractive, but still a challenge.[2] For example, nanoscale zerovalent iron (nZVI) could reductively remove various organic (e.g., chlorinated hydrocarbons) and inorganic (e.g., nitrate, chromate, perchlorate, metal ions) pollutants, and therefore be widely used for the remediation of contaminated groundwater and soil.[3,4] However, the reductive removal of organic pollutants with nZVI suffers from time-consuming and incomplete mineralization in some cases.[3,4]

In comparison with anaerobic removal of organic pollutants, nZVI could also activate molecular oxygen in air to produce reactive oxygen species (ROSs), including hydrogen peroxide (H_2O_2), superoxide radical ($\bullet O_2^-$), and hydroxyl radical ($\bullet OH$), which are capable of oxidizing contaminants that cannot be removed by nZVI reductively.[5−7] Obviously, the combination of abundant iron and molecular oxygen in air is highly desirable for pollutant control and environmental remediation in view of economical and environmental points and therefore attracts much attention. For instance, Waite's group reported that carbothiolate herbicide and molinate could be effectively degraded by an oxidative pathway in oxic solutions containing nanoscale zerovalent iron particles at initial pH of 4−8.1.[8,9] Cheng and his co-workers combined zerovalent iron, ethylenediaminetetraacetic acid, and air to develop an organic pollutant degradation system, which could nonselectively and deeply oxidize various compounds including 4-chlorophenol, pentachlorophenol, phenol, and malathion to low molecular weight acids and CO_2 at pH 5.5 under ambient conditions.[10] Sedlak's group found that organic ligands could enhance reactive oxidant generation by nZVI and molecular oxygen at near circumneutral pH,[5] and then systematically studied factors affecting the yield of oxidants, as well as quantified the oxidizing capacity of nZVI at acid or weak basic pH conditions.[7,11] In despite of these advances, the aerobic pollutant removal with nZVI is far less studied than those under anaerobic condition, hindering the environmental application of nZVI.

During the synthesis, drying, storage, shipping, and application processes, nZVI could be easily oxidized when exposed to the atmosphere and/or water due to its ultrafine size and high reactivity, resulting in the formation of iron oxide shell outside nanosized iron core. The oxide shell could protect nZVI from further oxidation, but might alternate surface reaction through specific interactions at the metal−oxide interface, thus influence their final reactivity. For instance,

Received: February 1, 2013
Revised: April 22, 2013
Accepted: April 25, 2013
Published: April 25, 2013

Tratnyek et al prepared two kinds of nZVI by the thermal reduction of goethite with H_2 (Fe^{H2}) and the reductive precipitation with borohydride (Fe^{BH}) and found the reductive products of carbon tetrachloride over Fe^{H2} consisting of α-Fe^0 and Fe_3O_4 particles were more favorable than that over core–shell Fe^{BH} with metallic Fe^0 particles and an oxide shell.[12] Signorini et al reported that iron–iron oxide core–shell nanoparticles exhibited size-dependent changes of local structure and oxidation state of the oxide shell upon oxygen exposure,[13] while Kuhn et al presented that core–shell iron–iron oxide nanoparticles possessed oxide shell dependent magnetic properties.[14] As for the aerobic degradation of organic pollutants, it is foreseeable that the oxide shell of nZVI would definitely influence the electron transfer from iron core to molecular oxygen and the subsequent molecular oxygen activation as well as the final oxidative degradation of organic pollutants, which is of great importance for the application of nZVI, but never reported previously to the best of our knowledge.

Our group previously reported the synthesis and environmental applications of core–shell $Fe@Fe_2O_3$ nanowires.[15−19] This special kind of nZVI was prepared by the reduction of ferric ions with sodium borohydride without any stirring because the disturbance of stirring would break the nanowires. These nanowires were able to efficiently degrade dye pollutants and pentachlorophenol in different Fenton systems. Meanwhile, these nZVI could be used to remove Cr(VI) from simulated wastewater.[15−20] In this study, we synthesize core–shell $Fe@Fe_2O_3$ nanowires with different iron oxide shell thickness through tuning water-aging time after the reduction of ferric ions with sodium borohydride without any stirring and investigate their reactivity toward organic pollutant removal with using air. The resulting samples were systematically characterized to reveal the physical insights on core–shell structure dependent reactivity of $Fe@Fe_2O_3$ nanowires.

■ EXPERIMENTAL SECTION

Chemicals. $NaBH_4$ (96%), $FeCl_3{\cdot}6H_2O$ (analytic reagent), Fe_3O_4 (99%), and $FeSO_4{\cdot}7H_2O$ (analytic reagent) were purchased from Sinopharm Chemical Reagent Co. Ltd., China. 4-chlorophenol (4-CP, >99%) was obtained from Acros, Pittsburgh, PA. *N*,*N*-dethyl-1,4-phenylene-diamine (DPD) was purchased from Alfa-Aesar, Ward Hill, MA. Horseradish peroxidase (POD, specific activity of 100 units m^{-1}), bipyridine (analytic reagent), terephthalic acid (TA) and 2-hydroxyterephthalic acid (TAOH) were purchased from Aladdin Chemistry Co. Ltd., China. Methanol (HPLC grade) was purchased from Tedia Company, Inc., USA. Xanthine, diethylenetriaminepentaacetic acid (DTPA), superoxide dismutase (SOD), and dimethyl sulfoxide (DMSO) were purchased from Sigma-Aldrich (St. Louis, MO). Spin trap 5-tert-butoxycarbonyl 5-methyl-1-pyrroline *N*-oxide (BMPO) was purchased from Bioanalytical Lab (Sarasota, FL); catalase and xanthine oxidase (XOD) came from Roche Applied Science (Indianapolis, IN). Deionized water was used throughout the experiments.

Samples Preparation. The core–shell $Fe@Fe_2O_3$ nanowires (CSFNs) were synthesized by the reduction of 0.01 mol/L of $FeCl_3{\cdot}6H_2O$ aqueous solution with 0.4 mol/L of $NaBH_4$ aqueous solution without any stirring.[15,16] Four kinds of CSNFs were synthesized by aging the freshly prepared nanowires in water for 0, 2, 4, and 6 h, which were denoted as CSFN-0, CSFN-2, CSFN-4, and CSFN-6, respectively. The detailed synthesis procedure is provided in the Supporting Information (SI). For comparison, Fe_2O_3 nanoplates were prepared according to a literature reported method.[21]

Aerobic Degradation of 4-CP. The reactivity of CSFNs toward organic pollutant removal with using air was evaluated with the aerobic degradation of 4-CP, which were carried out in 25 mL conical beakers at room temperature of about 25 °C. The initial pH of 4-CP solution was 6.0 without any adjusting. To initiate a reaction, 0.112 g of CSFNs was added to a 10 mL stock solution containing of 1.1 mmol/L of 4-CP under air bubbling with a flow of 1.5 L/min. In some cases, the initial pH of 4-CP solution was adjusted to 4.0 and 8.0 with 0.1 mol/L of H_2SO_4 and 0.1 mol/L of NaOH, respectively. For comparison, the anaerobic degradation of 4-CP was conducted under Ar gas bubbling with a flow of 1.5 L/min. The aerobic degradation of 4-CP in the presence of ferrous ions, or commercial Fe_3O_4, or Fe_2O_3 nanoplates, or ferrous ions and Fe_2O_3 nanoplates was also investigated. Samples were collected at regular intervals using a 2 mL syringe and filtered immediately through a 0.22 μm nylon syringe filter for high performance liquid chromatography (HPLC, Agilent TC-C18 reverse phase column, injection volume: 10 μL, water: methanol = 40%: 60%, column temperature: 30 °C, flow rate: 0.7 mL/min, detection wavelength: 270 nm) analysis immediately. All the degradation experiments were replicated for three times.

Analytic Methods. The total organic carbon (TOC) concentration was analyzed by a Shimadzu TOC-V CPH analyzer after filtration through 0.22 μm filter. Hydrogen peroxide was analyzed using the DPD method developed by Bader et al.[22] Typically, 0.4 mL of phosphate buffer solution (pH 6) and 0.1 mL of 0.01 mol/L bipyridine solution were premixed in a quartz cell, followed by the addition of 2 mL of the sample, and 30 μL of 1% DPD reagent in 0.1 mol/L H_2SO_4, and 30 μL of POD reagent successively. The absorbance at 551 nm was measured after the addition of the POD. Terephthalic acid (TA) was used as the fluorescent probe for the detection of hydroxyl radicals.[23] 2-hydroxyterephthalic acid (TAOH), which is the fluorescent product of the reaction of TA with •OH, has a strong fluorescent emission around 426 nm when excited at 312 nm. Fluorescence spectra of the supernatant liquid were measured with a fluorescence spectrophotometer (Cary Eclipse Fluorescent Spectrometer, FL1008M018). In a typical process, an aqueous solution with 0.01 mol/L of NaOH and 0.5 mmol/L of TA was prepared and then reacted with 2 mL of sample solution for 10 min the subsequent fluorescence measurements. The amount of produced TAOH was determined by the fluorescence intensity. The ferrous ion concentrations in the solution were measured by a modified 1,10-phenanthroline method at a wavelength of 510 nm using a UV–vis spectrophotometer (U-3310, HITACHI).[24] In a typical process, aqueous samples were added to 1 mL of 1, 10-phenanthroline (2 g/L) in a 1 cm quartz cell, deionized water was added to make the final volume of 3 mL. The absorbance was measured at λ = 510 nm, which is the maximal adsorption of Fe(II)-1,10-phenanthroline complex. Electron spin resonance (ESR) spectra were obtained with a Bruker EMX ESR Spectrometer (Billerica, MA) at room temperature. Fifty microliter aliquots of control or sample solutions were put in glass capillary tubes with internal diameters of 1 mm and sealed. The capillary tubes were inserted into the ESR cavity, and the spectra were recorded at selected times. The ESR spectra were recorded at 2 min.

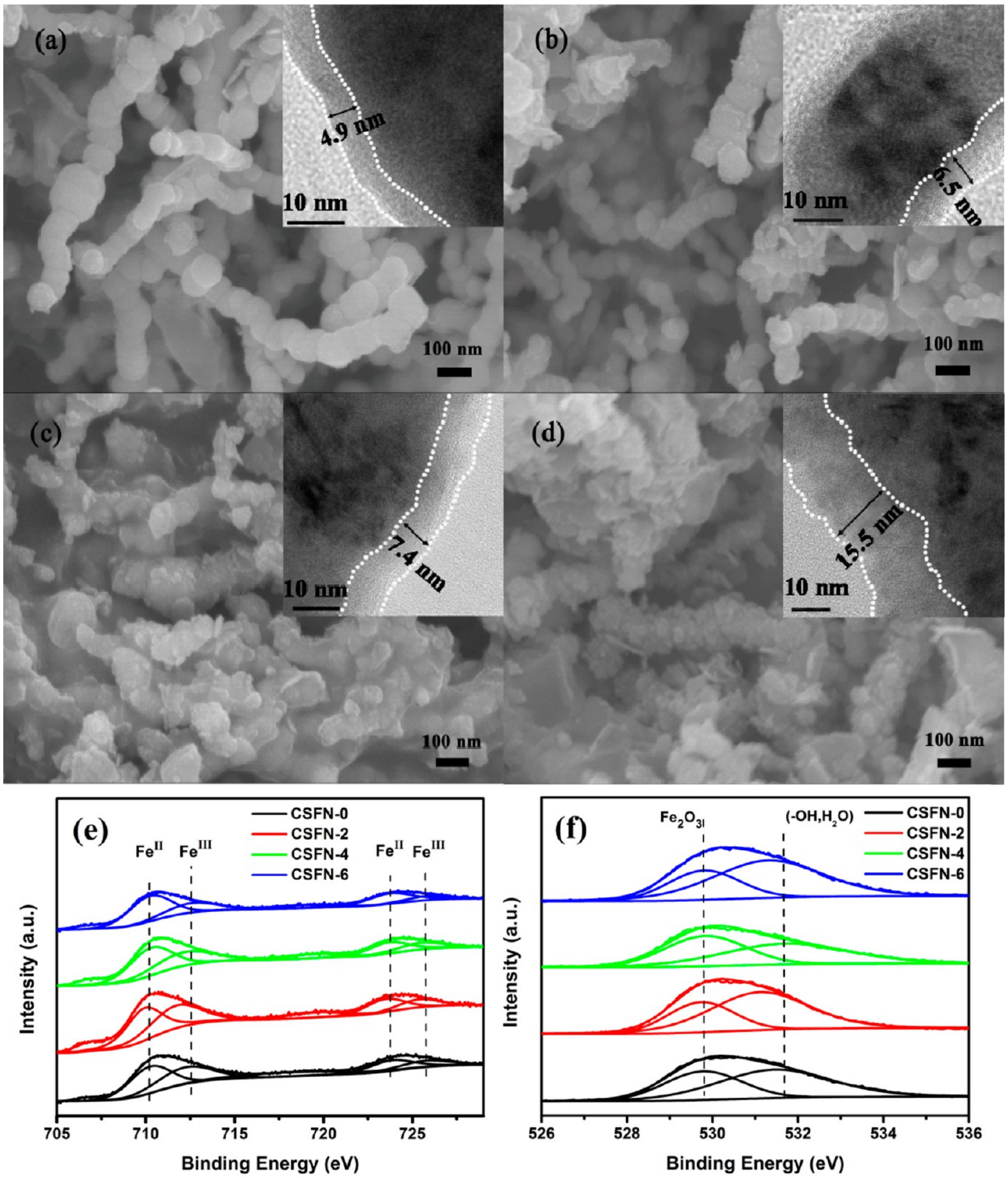

Figure 1. SEM/HRTEM images and XPS spectra of the as-prepared core−shell Fe@Fe_2O_3 nanowires. SEM images: (a) CSFN-0; (b) CSFN-2; (c) CSFN-4; and (d) CSFN-6. Corresponding HRTEM images: (inset in Figure 1a) CSFN-0; (inset in Figure 1b) CSFN-2; (inset in Figure 1c) CSFN-4; and (inset in Figure 1d) CSFN-6. XPS spectra: (e) high resolution spectra of Fe 2p, and (f) high resolution spectra of O1s.

RESULTS AND DISCUSSION

Characterization of CSFNs. The fours samples were analyzed using XRD (Figure S1, SI). An obvious diffraction peak at 2θ value of 44.9°, which matches well with the standard pattern of Fe^0 (JCPDS, file No. 87-722), was observed in the four CSFNs samples. The Fe^0 peak intensity of the CSFNs samples became slightly weaker with aging. The diffraction peak at 2θ values of 35.6° related to the standard patterns of Fe_2O_3 was not observed for all the CSFNs samples because of the amorphous nature of Fe_2O_3 according to our previous study.[15−19] The formation of amorphous Fe_2O_3 shell was confirmed by Raman spectra (Figure S2 in the SI). The bands at 222 and 498 cm^{-1}, and 288, 406, and 604 cm^{-1} appeared in the samples are ascribed to the A_{1g} stretching and E_g bending modes of Fe_2O_3, respectively.[25]

SEM examination revealed that the CSFN-0 and CSFN-2 were of abundant necklace-like nanowires with several tens of micrometers in length, whereas the CSFN-4 and CSFN-6, respectively, consisted of aggregated nanowires covered with many irregular nanoparticles and some plate-like nanoparticles (Figure 1), suggesting the aging process could result in surface changes of nanowires. The TEM images of CSFNs confirmed the existence of nanowires of 50−100 nm in width in all the four samples, whereas the nanowires were of iron nanoparticles core surrounded by a layer of iron oxide shell (Figure S3 in the SI), consistent with our previous reports.[15] The core−shell structures of the CSFNs were confirmed by HRTEM analysis (inset of Figure 1). The cores are made of crystalline nanoparticles and the shells are amorphous in the nature, which are consistent with XRD results. The oxide shells of

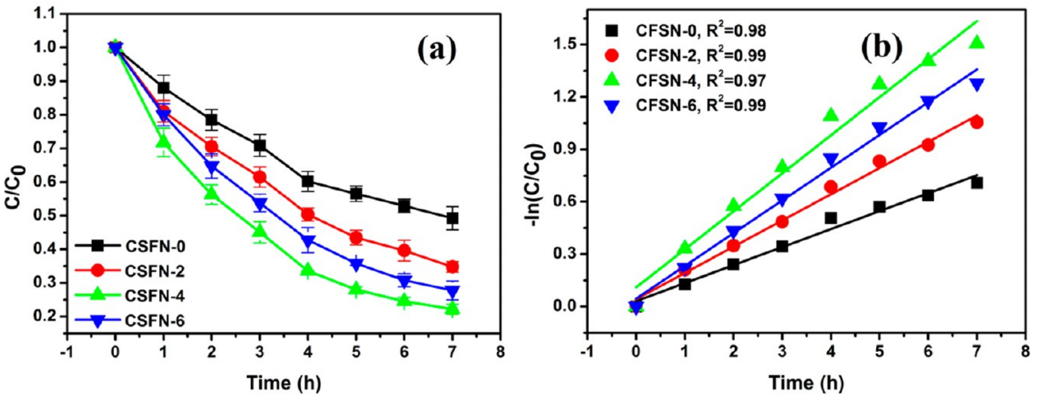

Figure 2. (a) The temporal concentration change of 4-CP as a function of reaction time during the aerobic degradation of 4-CP over CSFNs; (b) plots of ln(C/C_0) versus time.

CSFN-0, CSFN-2, CSFN-4, and CSFN-6 are, respectively, 4.9, 6.5, 7.4, and 15.5 nm in thickness, revealing that more iron oxide shell could be generated with prolonging water aging time because of the reactions of Fe^0 core with dissolved oxygen/water in the solution.

The composition of as-prepared CSFNs was further analyzed using X-ray photoemission spectroscopy (XPS) technique. The survey XPS spectra reveal that the synthesized CSFNs are composed of elements of Fe, O, and C (Figure S4a in the SI). The C 1s peak at 284.5 eV could be attributed to the adventitious carbon on the surface of the sample. No other C 1s peak could be observed in the high resolution C 1s XPS spectra (Figure S4b in the SI), indicating nonexistence of carbonaceous impurity in CSFNs. We found that various iron in nature of Fe^0, Fe^{II}, and Fe^{III} coexisted in the as-prepared CSFNs. The strong peak at 710.4 eV, the satellite signal at 719.2 eV, and the shoulder peak at 724.4 eV in the high-resolution spectra are assigned to Fe 2p (Figure 1e).[26−28] A peak at a low binding energy of 706.9 eV could be ascribed to Fe^0. The calculation of the peak area in Fe 2p core level spectra gave a ratio of ferrous iron to total iron (Fe^{II}/Fe_{total}) and ferric iron to total iron (Fe^{III}/Fe_{total}) (Table S1 in the SI). It was observed that the value of Fe^{III}/Fe_{total} increased from 0.323 to 0.384 with the water-aged time from 0 to 6 h, confirming that more amorphous Fe_2O_3 shell formed during the aging. Interestingly, the ratio of Fe^{II}/Fe_{total} for the CSFNs also increased from 0.263 to 0.312 with the water-aged time from 0 to 6 h, indicating that the amount of ferrous ions adsorbed on the surface increased with prolonging aging time. In the aging process, Fe^0 could react with dissolved oxygen and/or water, resulting in the formation of amorphous iron oxide shell as well as the leakage of ferrous ions into the solution. The leached ferrous ions would then be absorbed on the surface of the CSFNs, increasing the concentration of ferrous ions in CSFNs. In addition, the high-resolution XPS spectra of O 1s could be fitted by two peaks at binding energies of 530.0 and 531.5 eV, respectively (Figure 1f). The dominant peak at 530.0 eV is ascribed to the lattice oxygen binding with Fe (Fe_2O_3), while the other peak at around 531.5 eV suggests the presence of −OH, and H_2O adsorbed on the surface.[15,25] Further investigation of the peak area in O 1s core level spectra gave a ratio of oxygen in oxides to total oxygen (O_{Fe2O3}/O_{total}) and surface absorbed oxygen species to total oxygen (O_{OH}/O_{total}) (Table S1 in the SI). The atomic ratio of O_{Fe2O3}/O_{total} in CSFNs increased steady from 0.392 (CSFN-0) to 0.405 (CSFN-6), confirming the formation of more Fe_2O_3 shell with prolonging aging time.

Aerobic Degradation of 4-CP over CSFNs. The reactivity of fours CSFNs samples was evaluated by the aerobic degradation of 4-CP at room temperature (Figure 2). 50.8% of 4-CP was removed over CSFN-0 in 7 h, while higher efficiencies of 65.2%, 77.8%, and 72.2% for CSFN-2, CSFN-4, and CSFN-6 were observed (Figure 2a). The aerobic degradation 4-CP over CSFNs was found to be a pseudofirst order kinetic process (Figure 2b). The degradation rate constants ($k_{4\text{-CP}}$) over the CSFN-0, CSFN-2, CSFN-4, and CSFN-6 were 0.10, 0.15, 0.22, and 0.19 h^{-1}, respectively (Table S2 in the SI). The degradation rate of 4-CP over the CSFN-4 was more than 2 times that over CSFN-0. These results suggest that water aging process could enhance aerobic degradation of 4-CP and there is an optimal aging time for the preparation of CSFNs with higher reactivity.

A control experiment showed that 4-CP could not be degraded in the absence of oxygen (Figure S5 in the SI), ruling out the direct reductive degradation of 4-CP. In addition, the pH of 4-CP solution increased slightly from an initial value of 6.0 to a final value of about 7.0 (Figure S6 in the SI), which is indicative of the consumption of H^+ during the aerobic degradation of 4-CP over CSFNs. TOC measurement results indicated that about 30% of 4-CP could be oxidized to CO_2 after 10 h of degradation, revealing the partial mineralization of 4-CP during its aerobic degradation over CSFNs (Figure S7 in the SI). GC-MS analysis revealed that intermediate products of p-benzoquinone, phenol, and hydroquinone were generated during the degradation of 4-CP (Figure S8 in the SI). The aerobic degradation of 4-CP over CSFNs involved the cleavage of bonds between the chlorine and carbon atom in the benzene ring by •OH radicals, as well as the partial direct dechlorination of 4-CP by $•O_2^-$ radicals (Figure S9 in the SI),[18] accompanying with the formation of Cl^- (Figure S10 in the SI).

The above results clearly demonstrated that 4-CP could be oxidatively degraded with air over CSFNs, involving a molecular oxygen activation process. So the aerobic degradation of 4-CP over CSFNs is thought to be related to the concentration of dissolved oxygen, the pH of the solution, and the reactivity of CSFNs. Since the concentration of dissolved oxygen and the initial pH were the same during all the degradation processes, the different aerobic degradation efficiencies of 4-CP might be ascribed to the reactivity of CSFNs. It is known that surface area could affect the reactivity of catalyst,[3] we therefore measured BET surface areas of the

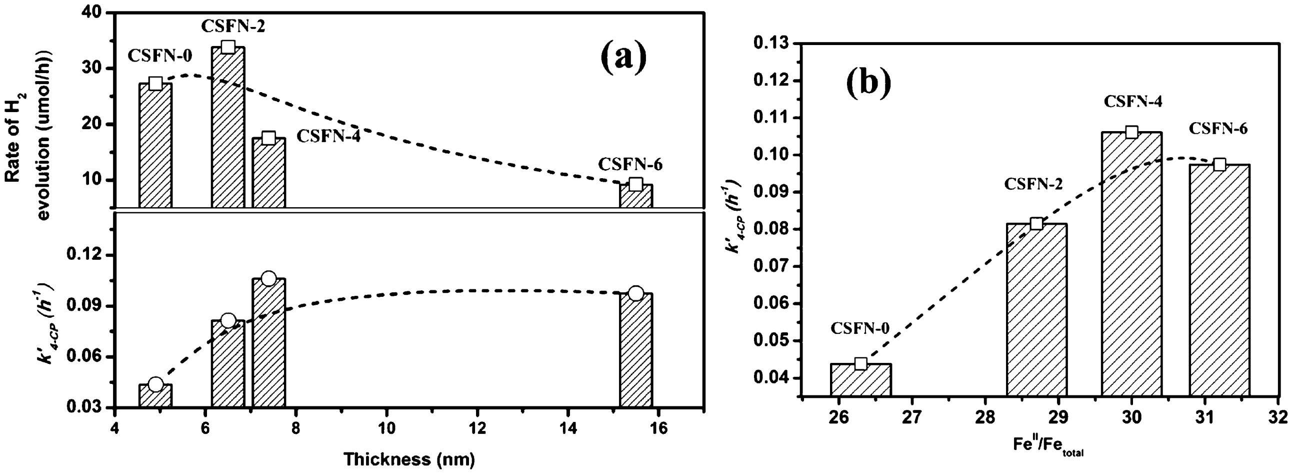

Figure 3. (a) The rates of hydrogen evolution (μmol·h^{-1}) over CSFNs in the absence of air and $k'_{4\text{-CP}}$ during the aerobic 4-CP degradation over CSFNs as a function of thickness (nm) of iron oxide shells; (b) $k'_{4\text{-CP}}$ during the aerobic 4-CP degradation over CSFNs as a function of the Fe^{II}/Fe_{total}. The dashed lines are the nonlinear fitting curve for the data, which represents the trend of the rates of hydrogen evolution and $k'_{4\text{-CP}}$ as a function of thickness of iron oxide shells, as well as $k'_{4\text{-CP}}$ during the aerobic 4-CP degradation over CSFNs as a function of the Fe^{II}/Fe_{total}, respectively.

four samples and compared their initial rate constants before and after being normalized to the BET specific surface area (Table S2 in the SI). The trend of normalized rate constants was the same as that of initial rate constants, suggesting that the different reactivity of CSFNs is not attributed to the surface area, but to the core–shell structure difference caused by the water-aging process.

To understand the core–shell structure dependent reactivity of $Fe@Fe_2O_3$ nanowires, we first need review the molecular oxygen activation on the catalyst surface of metallic iron. The oxidation of Fe^0 to ferrous ions is thought to be accompanied with the two-electron transfer to O_2 to generate H_2O_2 (eq 1), which would react with ferrous ions to produce •OH with strong oxidative ability under acidic to neutral pH conditions (eq 2).[7] This two-electron reduction molecular oxygen activation process is driven by the electron transfer from iron core of CSFNs to the surface of iron oxide shell, where the electrons could be captured by electrophilic molecular oxygen adsorbed on the surface of iron oxide shell.

$$Fe^0 + O_2 + 2H^+ \rightarrow Fe^{2+} + H_2O_2 \qquad (1)$$

$$Fe^{2+} + H_2O_2 \rightarrow Fe^{3+} + \bullet OH + OH^- \qquad (2)$$

Obviously, the iron oxide shell would affect the electron transfer process. Electron microscopy observation revealed that the thickness of iron oxide shell increased with prolonging water aging time (Figure 1), which could block the electron transfer. We found the ability of CSFNs to reduce water to hydrogen under argon atmosphere gradually declined (Figure S11 in the SI) and the hydrogen generation rates were inversely correlated to the thickness of iron oxide shell (Figure 3a), confirming the blocking of electron transfer because of incrassated iron oxide shell. However, the aerobic 4-chlorophenol removal reactivity of $Fe@Fe_2O_3$ nanowires first increased with iron oxide shell thickness increase and then decreased, while the sample obtained with 4 h of aging exhibited the highest activity. It is known that acid or basic condition could reduce or increase the thickness of iron oxide shell, respectively.[29] We interestingly found the aerobic degradation of 4-CP over the CSFN-4 decreased at either acid (pH 4.0) or basic condition (pH 8.0) (Figure S12 in the SI), suggesting the aerobic 4-chlorophenol removal reactivity of $Fe@Fe_2O_3$ nanowires strongly depends on the thickness of the iron oxide shell. Obviously, this structure dependent reactivity could not be well explained by the two-electron reduction molecular oxygen activation by nZVI. Therefore, a new molecular oxygen activation pathway is thought to take place during the aerobic degradation of 4-CP over CSFNs besides two electron reduction molecular oxygen activation pathway via the electron transfer from iron core to iron oxide shell of CSFNs.

It was reported that ferrous ions bound on the surface of iron oxide could activate molecular oxygen via single-electron reduction pathway to produce superoxide radicals.[30−35] For example, Pecher's group demonstrated that the uptake of ferrous iron by iron oxides resulted in the formation of various ROSs capable of reducing polyhalogenated methanes and indicated that the single-electron transfer pathway predominated in the ferrous iron and iron oxides system at alkaline pH values.[34] While Coughlin and Stone proposed the redox reaction between adsorbed Fe(II) and the underlying Fe oxide ($\equiv Fe^{III}OH$) (eqs 3-5), where hydroxyl ligands at the oxide surface could act as sigma donor ligands and increase the electron density of the Fe(II) species, while the presence of surface bound Fe(II) species ($\equiv Fe^{III}OFe^{II}OH/\equiv Fe^{II}OFe^{III}OH$) would accelerate molecular oxygen activation (eq 5).[30] Since the aforementioned XPS analysis revealed that the amount of ferrous ions on the iron oxide surface increased with prolonging aging time, we assume that ferrous ions bound on iron oxide shell of CSFNs would be another molecular oxygen activation pathway to enhance the generation of ROSs for the subsequent oxidative degradation of 4-CP.

$$\equiv Fe^{III}OH + Fe(II) + H_2O \rightarrow \equiv Fe^{III}OFe^{II}OH + 2H^+ \qquad (3)$$

$$\equiv Fe^{III}OFe^{II}OH \rightarrow \equiv Fe^{II}OFe^{III}OH \qquad (4)$$

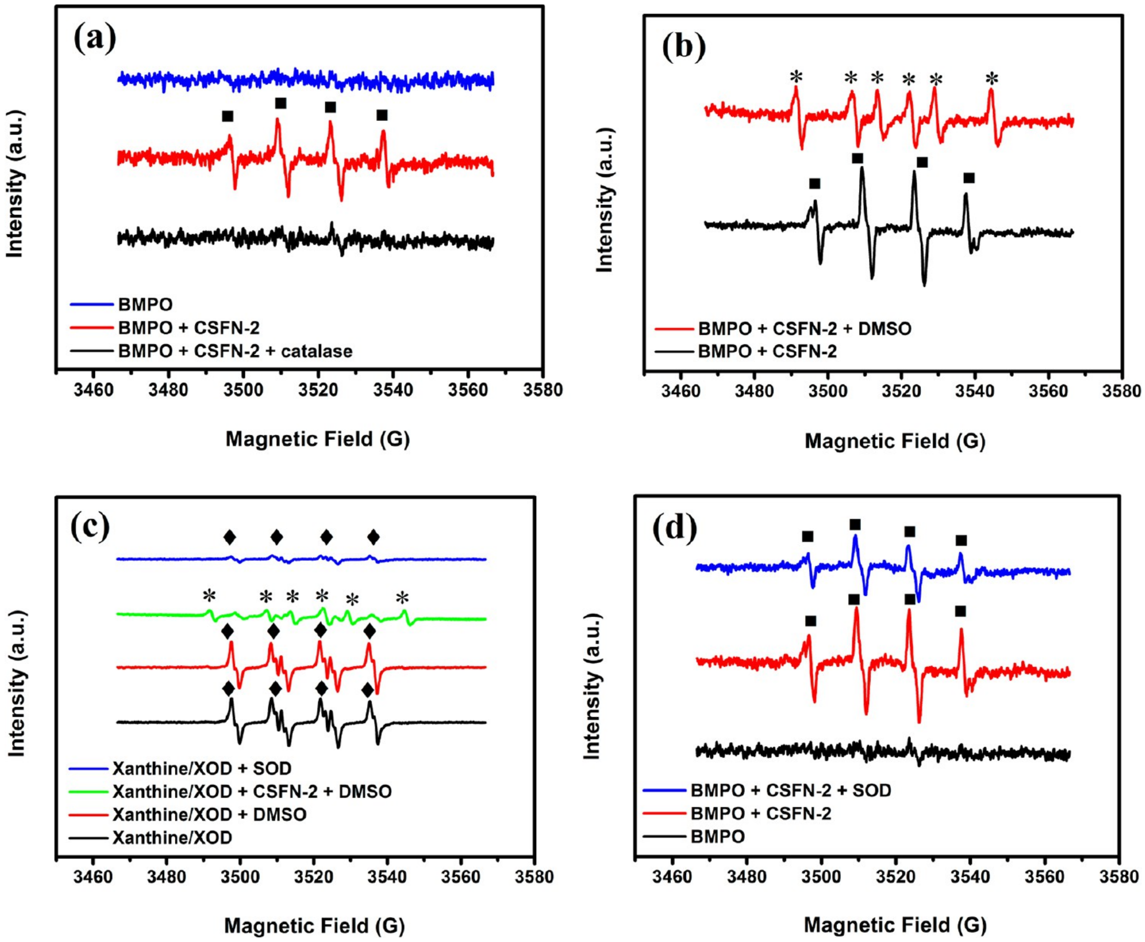

Figure 4. (a) ESR spectra obtained from samples containing 25 mM BMPO (black curve), 25 mM BMPO + 0.1 mg/mL CSFN-2 supernate (red curve), and 25 mM BMPO + 0.1 mg/mL CSFN-2 supernate +20 U/mL catalase (blue curve); (b) ESR spectra obtained from samples containing 25 mM BMPO (black curve), 25 mM BMPO, and 0. One mg/mL CSFN-2 without (red curve) and with 100 U/ml SOD (blue curve); (c) ESR spectra from samples containing 25 mM BMPO + 0.1 mg/mL CSFN-2 in water (red curve) or in 20% DMSO (black curve); (d) ESR spectra of BMPO/•OOH and superoxide radical scavenging activity of CSFN-2. Samples contained 25 mM BMPO, 10 mM pH 7.4 PBS buffer, 1 mM Xanthine, 0.05 mM DTPA, 0.2 U/mL XOD (black curve, control), control +20% DMSO (red curve), control +0.1 mg/mL CSFN-2 with 20% DMSO (green curve); control +1 U/mL SOD (blue curve).

$$\equiv \mathrm{Fe^{III}OFe^{II}OH}/ \equiv \mathrm{Fe^{II}OFe^{III}OH} + \mathrm{O_2} \rightarrow \mathrm{Fe(III)} + \bullet \mathrm{O_2}^- \quad (5)$$

To validate this assumption, two control experiments of aerobic degradation of 4-CP in the presence of ferrous iron and/or Fe_2O_3 nanoplates were performed (Figure S13 in the SI). It was found that the degradation of 4-CP was negligible in the presence of ferrous iron (5.3%) or Fe_2O_3 nanoplates (4.1%). However, a much higher aerobic degradation (19.8%) of 4-CP was observed in the presence of ferrous ions and Fe_2O_3, suggesting that the interaction between ferrous ions and iron oxides could contribute to the aerobic degradation of 4-CP via the single-electron reduction pathway of molecular oxygen activation. We also checked the changes of normalized degradation rates $k'_{4\text{-CP}}$ with ferrous ions contents in CSFNs and interestingly found the $k'_{4\text{-CP}}$ were positively correlated to the amount of Fe(II) bound to the iron oxide shell (Figure 3b), confirming more surface bound ferrous ions could favor the single-electron molecular oxygen activation, which could counteract the negative effect of incrassated iron oxide shell on the two electron reduction molecular oxygen activation. We also found that the degradation of 4-CP was negligible in the presence of commercial Fe_3O_4 (Figure S13 in the SI), revealing that the higher reactivity in aged CSFNs in this study was not attributed to the amorphous magnetite possibly formed on the surface of CSFNs, but to the surface bound ferrous ions.

5-tert-butoxycarbonyl 5-methyl-*N*-oxide (BMPO), which was often used as spin traps to capture hydroxyl radical and superoxide, was chosen to investigate the ROSs generated by CSFNs and molecular oxygen. Figure 4a shows the ESR spectra obtained from the sample containing BMPO in the absence and presence of CSFN-2. No characteristic ESR spectra for spin adduct attributable to hydroxyl radical and superoxide was observed in the absence of CSFN-2. A four-line ESR spectrum with relative intensities of 1:2:2:1 and hyperfine splitting parameters of $a^N = 13.56$, $a^{\beta}H = 12.30$, $a^{\gamma}H = 0.66$ appeared upon the addition of CSFN-2, which is characteristic for spin adduct BMPO/•OH (marked with square).[36] This result confirms that hydroxyl radicals could be produced from the CSFNs aqueous suspensions. The hydroxyl radicals induced by CSFN-2 were almost totally inhibited by catalase, which is the enzyme can catalyze the decomposition of hydrogen peroxide to water and oxygen quickly. This implied that hydrogen peroxide is an intermediate for the production of hydroxyl radicals via the Fenton reaction between hydrogen peroxide and ferrous ions.[8,37] The addition of 20% DMSO, a commonly recognized hydroxyl radical scavenger, reduced the BMPO/•OH ESR signal intensity and resulted in the formation of new ESR spectrum characteristic for spin adduct of BMPO/•CH_3 (marked with asterisk), evidencing indirectly the generation of hydroxyl radicals in CSFN-2 suspensions (Figure 4b). As Fe@Fe_2O_3 nanowires had better dispersion in DMSO than in water, we thus conducted further ESR experiment using Fe@Fe_2O_3 suspension in DMSO.

Although some researchers have reported the generation of superoxide in Fe based nanoparticles system,[35] we did not observe the typical ESR spectrum for spin adduct BMPO/•O_2^-, which is the most acceptable and direct evidence of superoxide. To check if superoxide is generated from the molecular oxygen activation by Fe@Fe_2O_3 nanowires, we turn to study the interaction between Fe@Fe_2O_3 nanowires and superoxide. Superoxide could be generated by the classic enzymatic reaction of xanthine and XOD, which was used to examine the superoxide scavenging activity of Fe_2O_3 nanoparticles.[35] Figure 4c shows the typical ESR spectrum of spin adduct BMPO/•OOH (marked with diamond) having four lines with relative intensities of 1:1:1:1 and hyperfine splitting parameters of $a_N = 13.4$, $a^{\beta}_H = 12.1$ in the aqueous solution of xanthine and XOD. It worthy noted that DMSO caused negligible effect on the superoxide products. However, after adding 0.1 mg/mL CSFN-2 (20% DMSO) suspension, the BMPO/•OOH ESR signal intensity decreased considerably, accompanying with the appearance of the signal of BMPO/•CH_3. As expected, the ESR signal intensity decreased greatly when 1 U/mL SOD was added to the aqueous solution of xanthine and XOD because of its ability to dismutate superoxide. These results indicated that Fe@Fe_2O_3 nanowires could not only scavenge the superoxide, but also may enhance the generation of hydroxyl radicals, proven by the formation of BMPO/•CH_3 signal. Further experiment was conducted to study the effect of SOD on the apparent BMPO/•OH ESR signal in CSFNs system (Figure 4d). The BMPO/•OH signal intensity decreased after the addition of SOD, providing an indirect evidence for the generation of superoxide in CSFNs system. The typical ESR spectrum of BMPO/•OOH was indistinctive in our work, which may be due to the strong intensity of BMPO/•OH signal and the superposition of BMPO/•OH and BMPO/•OOH signals. The reason for no ESR signal of BMPO/•O_2^- in the Fe@Fe_2O_3 nanowires aqueous suspension might be attributed to the superoxide scavenging activity of Fe_2O_3 nanoparticles on the surface of Fe@Fe_2O_3 nanowires and/or the fast reactions between superoxide and ferrous irons (eq 6) or ferric ions (eq 7).[38]

$$\mathrm{Fe(II)} + \bullet O_2^- + H^+ \rightarrow \mathrm{Fe(III)} + H_2O_2 \quad k = 1 \times 10^7 \tag{6}$$

$$\mathrm{Fe(III)} + \bullet O_2^- \rightarrow \mathrm{Fe(II)} + O_2 \quad k = 5 \times 10^7 \tag{7}$$

The active species trapping experiments were then carried out by adding isopropyl alcohol (•OH scavenger), catalase (H_2O_2 scavenger), and superoxide dismutase (SOD, •O_2^- scavenger) as scavengers to the aerobic 4-CP degradation solution in presence of the CSFN-4 (Figure S14 in the SI). The addition of these three scavengers could inhibit the aerobic degradation of 4-CP (Figure S14a in the SI), confirming the involving of •O_2^-, H_2O_2, and •OH species in the aerobic degradation of 4-CP over Fe@Fe_2O_3 nanowires. Moreover, the amount of •OH generated over different CSFNs was quantified by the fluorescence method (Figure S14b in the SI), revealing that CSFN-4 could generate more •OH radicals than other samples via molecular oxygen activation, which is consistent with the results of aerobic 4-CP degradation.

Scheme 1. (a) Formation of CSFNs with prolonging water aging time; (b) possible molecular oxygen activation pathway over the Fe@Fe_2O_3 nanowires

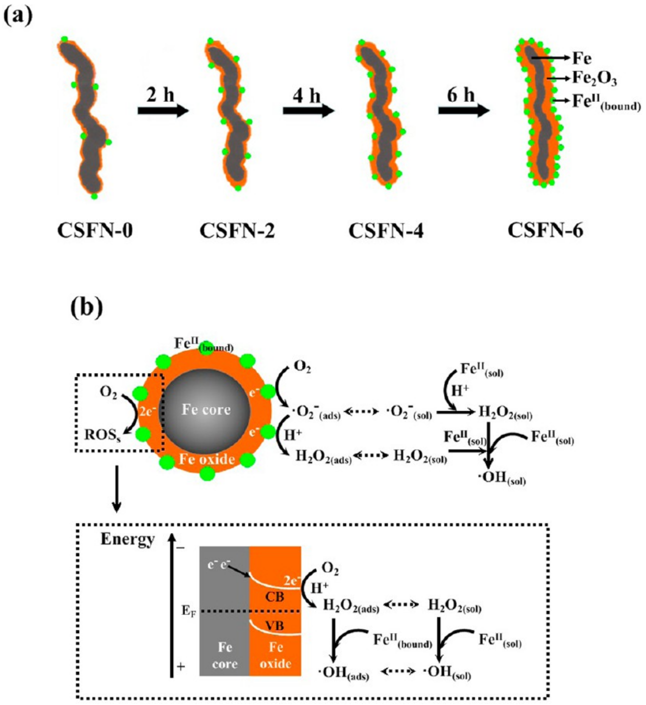

On the basis of all the above results and discussions, a possible mechanism for the formation of core−shell structure and the structure-dependent aerobic catalytic degradation of 4-CP over CSFNs is proposed in Scheme 1. As shown in Scheme 1a, iron oxide was initially generated and grown on the surface of iron nanowires when freshly prepared iron nanowires were exposed to water, resulting in the formation of core−shell structure. With prolonging aging time, the iron core decreased, accompanying with iron oxide shell growth and ferrous ions leaching. These ferrous ions would be adsorbed on the iron oxide shell subsequently, leading to in situ formation of surface bound ferrous ions ($Fe^{(II)}{}_{bound}$). The amount of surface bound ferrous ions would increase with prolonging aging time. As for the aerobic degradation of 4-CP over CSFNs (Scheme 1b), the first step was the oxidation of nanosized iron core via electron transfer from iron core to the surface of iron oxide shell along the conduction band. The electron transfer was spontaneously driven by lower work function (4.5 eV) of Fe^0 than that (5.6 eV) of Fe_2O_3. Therefore, the Ohmic contact between iron core and iron oxide shell would result in band bending and electrons flow from the iron core to the conduction band of the Fe_2O_3 shell to lower their energies until the positions of their Fermi energy levels are adjusted to the same value.[39,40] Since the conduction band position of iron oxide is 0.26 V vs NHE, more positive than the reduction potential (−0.33 V vs NHE) of O_2/•O_2^-, but more negative than the reduction potential (0.69 V vs NHE) of O_2/H_2O_2, the electrons on the conduction band of iron oxide would only reduce molecular oxygen absorbed on the CSFNs surface via a two-electron reduction pathway to generate H_2O_2.[7] As the ferrous ions leached into the aqueous solution during the process[38] (Figure S15 in the SI), the generated H_2O_2 would then react with both dissolved and surface bound ferrous ions to produce hydroxyl radicals for the oxidative degradation of 4-CP. In view of the semiconducting characteristic of iron oxide, the electron transfer from iron core to iron oxide shell and the subsequent electron transportation among the iron oxide shell would become slower with the shell thickness increase and even be blocked gradually (as revealed by hydrogen generation in Figure 3a), inhibiting the two-electron reduction molecular oxygen activation pathway. On the contrary, the surface bound ferrous ions on the iron oxide shell could then initiate the single-electron reduction of oxygen to activate molecular oxygen for the generation of superoxide radicals, H_2O_2 and hydroxyl radicals to further oxidize 4-CP. With prolonging aging time, more surface bound ferrous ions could form and then promote the single-electron molecular oxygen activation pathway to generate more ROSs, which could counteract the negative effect of incrassated iron oxide shell on the two electron reduction molecular oxygen activation. The combination of two kinds of molecular oxygen activation pathway could well explain the core−shell structure dependent aerobic oxidative reactivity of $Fe@Fe_2O_3$ nanowires. See Scheme 1.

■ ASSOCIATED CONTENT

Ⓢ Supporting Information

Additional descriptions, figures, and tables as mentioned in the text. This material is available free of charge via the Internet at http://pubs.acs.org.

■ AUTHOR INFORMATION

Corresponding Author

*Phone/Fax: +86-27-6786 7535; e-mail: zhanglz@mail.ccnu.edu.cn.

Notes

The authors declare no competing financial interest.

■ ACKNOWLEDGMENTS

This work was supported by National Science Foundation of China (Grants 21073069, 91023010, 21173093, and 21177048), and Changjiang Scholars and Innovative Research Team in University (Grant IRT0953), and a regulatory science grant under the FDA Nanotechnology CORES Program and by the Office of Cosmetics and Colors, CFSAN/FDA (W.H and J.Y). This article is not an official US Food and Drug Administration (FDA) guidance or policy statement. No official support or endorsement by the US FDA is intended or should be inferred.

■ REFERENCES

(1) Grundl Timothy, J.; Haderlein, S.; Nurmi James, T.; Tratnyek Paul, G., Introduction to aquatic redox chemistry. In *Aquatic Redox Chemistry*; Tratnyek, P. G., Grundl, T., Haderlein, S., Eds.; 2011; Vol.*1071*, pp 1−14. ISBN 13: 9780841226524.

(2) Hippeli, S.; Elstner, E. F. Transition metal ion-catalyzed oxygen activation during pathogenic processes. *FEBS Lett.* **1999**, *443*, 1−7.

(3) Tanapon, P.; Daniel, S.; Mark, L.; June, Y.; Steven, A. P.; Gregory, V. L., Treatability study for a TCE contaminated area using nanoscale- and microscale-zerovalent iron particles: Reactivity and reactive life time. In *Environmental Applications of Nanoscale and Microscale Reactive Metal Particles*; Geiger, C. L., Carvalho-Knighton, K. M. Eds.; 2009; Vol. *1027*, pp 183−202. ISBN13: 9780841269927.

(4) Phillips, D. H.; Nooten, T. V.; Bastiaens, L.; Russell, M. I.; Dickson, K.; Plant, S.; Ahad, J. M. E.; Newton, T.; Elliot, T.; Kalin, R. M. Ten year performance evaluation of a field-scale zero-valent iron permeable reactive barrier installed to remediate trichloroethene contaminated groundwater. *Environ. Sci. Technol.* **2010**, *44*, 3861−3869.

(5) Keenan, C. R.; Sedlak, D. L. Ligand-enhanced reactive oxidant generation by nanoparticulate zero-valent iron and oxygen. *Environ. Sci. Technol.* **2008**, *42*, 6936−6941.

(6) Que, L.; Tolman, W. B. Biologically inspired oxidation catalysis. *Nature* **2008**, *455*, 333−340.

(7) Keenan, C. R.; Sedlak, D. L. Factors affecting the yield of oxidants from the reaction of nanoparticulate zero-valent iron and oxygen. *Environ. Sci. Technol.* **2008**, *42*, 1262−1267.

(8) Joo, S. H.; Feitz, A. J.; Waite, T. D. Oxidative degradation of the carbothioate herbicide, molinate, using nanoscale zero-valent iron. *Environ. Sci. Technol.* **2004**, *38*, 2242−2247.

(9) Joo, S. H.; Feitz, A. J.; Sedlak, D. L.; Waite, T. D. Quantification of the oxidizing capacity of nanoparticulate zero-valent iron. *Environ. Sci. Technol.* **2004**, *39*, 1263−1268.

(10) Noradoun, C.; Engelmann, M. D.; McLaughlin, M.; Hutcheson, R.; Breen, K.; Paszczynski, A.; Cheng, I. F. Destruction of chlorinated phenols by dioxygen activation under aqueous room temperature and pressure conditions. *Ind. Eng. Chem. Res.* **2003**, *42*, 5024−5030.

(11) Keenan, C. R.; Goth-Goldstein, R.; Lucas, D.; Sedlak, D. L. Oxidative stress induced by zero-valent iron nanoparticles and Fe(II) in human bronchial epithelial cells. *Environ. Sci. Technol.* **2009**, *43*, 4555−4560.

(12) Nurmi, J. T.; Tratnyek, P. G.; Sarathy, V.; Baer, D. R.; Amonette, J. E.; Pecher, K.; Wang, C.; Linehan, J. C.; Matson, D. W.; Penn, R. L.; Driessen, M. D. Characterization and properties of metallic iron nanoparticles: Spectroscopy, electrochemistry, and kinetics. *Environ. Sci. Technol.* **2004**, *39*, 1221−1230.

(13) Signorini, L.; Pasquini, L.; Savini, L.; Carboni, R.; Boscherini, F.; Bonetti, E.; Giglia, A.; Pedio, M.; Mahne, N.; Nannarone, S. Size-dependent oxidation in iron/iron oxide core-shell nanoparticles. *Phys. Rev. B* **2003**, *68*, 195423.

(14) Kuhn, L. T.; Bojesen1, A.; Timmermann1, L.; M., N. M.; Mørup, S. Structural and magnetic properties of core−shell iron−iron oxide nanoparticles. *J. Phys.: Condens. Matter* **2002**, *14*, 13551−13567.

(15) Lu, L.; Ai, Z.; Li, J.; Zheng, Z.; Li, Q.; Zhang, L. Synthesis and characterization of Fe-Fe_2O_3 Core-shell nanowires and nanonecklaces. *Cryst. Growth Des.* **2007**, *7*, 459−464.

(16) Ai, Z.; Lu, L.; Li, J.; Zhang, L.; Qiu, J.; Wu, M. $Fe@Fe_2O_3$ core-shell nanowires as iron reagent. 1. Efficient degradation of rhodamine B by a novel sono-Fenton process. *J. Phys. Chem. C* **2007**, *111*, 4087−4093.

(17) Ai, Z.; Lu, L.; Li, J.; Zhang, L.; Qiu, J.; Wu, M. $Fe@Fe_2O_3$ core-shell nanowires as the iron reagent. 2. An efficient and reusable sono-Fenton system working at neutral pH. *J. Phys. Chem. C* **2007**, *111*, 7430−7436.

(18) Ai, Z.; Mei, T.; Liu, J.; Li, J.; Jia, F.; Zhang, L.; Qiu, J. $Fe@Fe_2O_3$ core-shell nanowires as an iron reagent. 3. Their combination with CNTs as an effective oxygen-fed gas diffusion electrode in a neutral electro-Fenton system. *J. Phys. Chem. C* **2007**, *111*, 14799−14803.

(19) Luo, T.; Ai, Z.; Zhang, L. $Fe@Fe_2O_3$ core-shell nanowires as iron reagent. 4. Sono-Fenton degradation of pentachlorophenol and the mechanism analysis. *J. Phys. Chem. C* **2008**, *112*, 8675−8681.

(20) Ai, Z.; Cheng, Y.; Zhang, L.; Qiu, J. Efficient removal of Cr(VI) from aqueous solution with $Fe@Fe_2O_3$ core-shell nanowires. *Environ. Sci. Technol.* **2008**, *42*, 6955−6960.

(21) Chen, L.; Yang, X.; Chen, J.; Liu, J.; Wu, H.; Zhan, H.; Liang, C.; Wu, M. Continuous shape- and spectroscopy-tuning of hematite nanocrystals. *Inorg. Chem.* **2010**, *49*, 8411−8420.

(22) Bader, H.; Sturzenegger, V.; Hoigné, J. Photometric method for the determination of low concentrations of hydrogen peroxide

peroxidase by the peroxidase catalyzed oxidation of N,N-diethyl-*p*-phenylenediamine (DPD). *Water Res.* **1988**, *22*, 1109−1115.

(23) Hirakaw, T.; Nosak, Y. Properties of $O_2^{\cdot-}$ and $OH^{\cdot}$formed in TiO_2 aqueous suspensions by photocatalytic reaction and the influence of H_2O_2 and some ions. *Langmuir* **2002**, *18*, 3247−3254.

(24) Dunnivant, F. M.; Schwarzenbach, R. P.; Macalady, D. L. Reduction of substituted nitrobenzenes in aqueous solutions containing natural organic matter. *Environ. Sci. Technol.* **1992**, *26*, 2133−2141.

(25) Zhou, X.; Lan, J.; Liu, G.; Deng, K.; Yang, Y.; Nie, G.; Yu, J.; Zhi, L. Facet-mediated photodegradation of organic dye over hematite architectures by visible light. *Angew. Chem., Int. Ed.* **2012**, *124*, 182−186.

(26) Cattaruzza, F.; Fiorani, D.; Flamini, A.; Imperatori, P.; Scavia, G.; Suber, L.; Testa, A. M.; Mezzi, A.; Ausanio, G.; Plunkett, W. R. Magnetite nanoparticles anchored to crystalline silicon surfaces. *Chem. Mater.* **2005**, *17*, 3311−3316.

(27) Mills, P.; Sullivan, J. L. A study of the core level electrons in iron and its three oxides by means of X-ray photoelectron spectroscopy. *J. Phys. D: Appl. Phys.* **1983**, *16*, 723−732.

(28) Teng, X.; Black, D.; Watkins, N. J.; Gao, Y.; Yang, H. Platinum-maghemite core-shell nanoparticles using a sequential synthesis. *Nano Lett.* **2003**, *3*, 261−264.

(29) Sato, N.; Noda, T.; Kudo, K. Thickness and structrue of passive films on iron in acidic and basic solution. *Electrochim. Acta* **1974**, *19*, 471−475.

(30) Coughlin, B. R.; Stone, A. T. Nonreversible adsorption of divalent metal ions (Mn^{II}, Co^{II}, Ni^{II}, Cu^{II}, and Pb^{II}) onto goethite: Effects of acidification, Fe^{II} addition, and picolinic acid addition. *Environ. Sci. Technol.* **1995**, *29*, 2445−2455.

(31) Gorski, C. A.; Nurmi, J. T.; Tratnyek, P. G.; Hofstetter, T. B.; Scherer, M. M. Redox behavior of magnetite: Implications for contaminant reduction. *Environ. Sci. Technol.* **2009**, *44*, 55−60.

(32) Gorski, C. A.; Handler, R. M.; Beard, B. L.; Pasakarnis, T.; Johnson, C. M.; Scherer, M. M. Fe atom exchange between aqueous Fe^{2+} and magnetite. *Environ. Sci. Technol.* **2012**, *46*, 12399−12407.

(33) Ona-Nguema, G.; Morin, G.; Wang, Y.; Foster, A. L.; Juillot, F.; Calas, G.; Brown, G. E. XANES evidence for rapid arsenic(III) oxidation at magnetite and ferrihydrite surfaces by dissolved O_2 via Fe^{2+}-mediated reactions. *Environ. Sci. Technol.* **2010**, *44*, 5416−5422.

(34) Pecher, K.; Haderlein, S. B.; Schwarzenbach, R. P. Reduction of polyhalogenated methanes by surface-bound Fe(II) in aqueous suspensions of iron oxides. *Environ. Sci. Technol.* **2002**, *36*, 1734−1741.

(35) Voinov, M. A.; Pagán, J. O. S.; Morrison, E.; Smirnova, T. I.; Smirnov, A. I. Surface-mediated production of hydroxyl radicals as a mechanism of iron oxide nanoparticle biotoxicity. *J. Am. Chem. Soc.* **2010**, *133*, 35−41.

(36) T, Z. H.; J, J.; H, Z.; H, K.; B, K. Synthesis and biochemical applications of a solid cyclic nitrone spin trap: A relatively superior trap for detecting superoxide anions and glutathiyl radicals. *Free Radic. Biol. Med.* **2001**, *3*, 599−606.

(37) Kang, S. H.; Choi, W. Oxidative degradation of organic compounds using zero-valent iron in the presence of natural organic matter serving as an electron shuttle. *Environ. Sci. Technol.* **2008**, *43*, 878−883.

(38) Brillas, E.; Sirés, I.; Oturan, M. A. Electro-Fenton process and related electrochemical technologies based on Fenton's reaction chemistry. *Chem. Rev.* **2009**, *109*, 6570−6631.

(39) Tang, D. M.; Liu, G.; Li, F.; Tan, J.; Liu, C.; Lu, G. Q.; Cheng, H.-M. Synthesis and photoelectrochemical property of urchin-like Zn/ZnO core−shell structures. *J. Phys. Chem. C* **2009**, *113*, 11035−11040.

(40) Batista, E. R.; Friesner, R. A. A self-consistent charge-embedding methodology for ab initio quantum chemical cluster modeling of ionic solids and surfaces: Application to the (001) surface of hematite (α-Fe_2O_3). *J. Phys. Chem. B* **2002**, *106*, 8136−8141.

NOTE ADDED AFTER ASAP PUBLICATION

This article was published ASAP on May 7, 2013, with minor text errors. The corrected version was published ASAP on May 9, 2013.